Preparation of Pseudotetragonal ZrO$_{0.75}$S and Its Electric Responses on Temperature and Frequency Related to Microstructural Relaxation

Young-A Ro, Sung-Jin Kim,[†] You-Kyung Lee,[†] and Chy Hyung Kim[*]

Department of Chemistry, Chongju University, Chongju 360-764, Korea
[†]Department of Chemistry, Ewha Woman's University, Seoul 120-750, Korea
Received July 3, 2001

Pseudotetragonal ZrO$_{0.75}$S whose space group is P2$_1$2$_1$2$_1$ was synthesized and the cell dimensions were a=5.110(2) Å, b=5.110(7) Å, and c=5.198(8) Å. The space group P2$_1$2$_1$2$_1$ seems to be resulted from lowering the symmetry of cubic ZrOS structure with P2$_1$3 space group by lattice distortion due to the oxygen defects. In the distorted structure, bond shortening between metal-nonmetal by reduction of cell volume and alternation of Zr-Zr distance were observed. Dielectric constant and loss data of the bulk material in temperature range -170 to 20 °C and frequency range 50 Hz to 1 MHz showed that there was dielectric transition at around -70 °C originated from the relaxation of Zr-S segment. Comparing with ZrO$_2$ exhibited the dielectirc constants, 9.0 at room temperature, ZrO$_{0.75}$S showed high dielectric constant, $k = 200.2$ at 100 kHz. The activation energy of relaxation time due to dielectric relaxation of Zr-S was 0.47 eV (11.3 kcal/mole). According to the impedance spectra, ZrO$_{0.75}$S showed more parallel circuit character between the resistance and capacitance components at the temperature (-70 °C) that the Zr-S dielectric relaxation was observed.

Keywords : ZrO$_{0.75}$S, Pseudotetragonal structure, Dielectric relaxation, Activation energy of relaxation time.

Introduction

Metal oxide and metal sulfide such as the ZrO$_2$ and ZrS$_2$ have different structures and different properties even though the oxygen and sulfur belong same group in periodic table. We know well the sulfur is larger in size, less electro-negative, and the d orbitals of sulfur are available for bonding. For example, the resistivity of ZrO$_2$ is 10^{14} Ω·cm and ZrS$_2$ is nearly metallic degenerate semiconductor[1] at room temperature. Therefore, it will be very interesting to study on the electrical behavior of Zr-O-S system which contains both oxygen and sulfur, and to compare it with insulating ZrO$_2$ system and semiconducting ZrS$_2$ system. ZrOS with cubic structure has been first prepared by passage of H$_2$S over Zr(SO$_4$)$_2$ at red heat[2] and by passing H$_2$S through a graphite tube containing ZrO$_2$ at 1300 °C.[3] Also, the synthesis of the tetragonal ZrOS has been reported[4] but no electrical properties of the material have been studied yet although electric properties of ZrO$_2$ and ZrS$_2$ have been well known.[5-9]

In this study, ZrO$_{0.75}$S with a pseudotetragonal lattice was synthesized by passing CS$_2$ vapor flow through a quartz tube containing ZrOCl$_2$ · 8H$_2$O at 400 °C. The structural variation will be discussed. Also, measurements of dielectric constant, loss and impedance in temperature range -170 to 20 °C and frequency range 50 Hz to 1 MHz were performed to investigate the dielectric relaxation induced by segmental fluctuation of the molecule, activation energy of the relaxation time, and the circuit character of the phase. To measure the dielectric constants of ZrO$_2$, both the forms of bulk and film were used. The film was prepared by sol-gel process, in which the films were grown layer-by-layer, by performing the hydrolysis and condensation reactions in separate steps.[10]

Experimental Section

Yellow powder of ZrO$_x$S ($0 < x < 1$) was synthesized by heating pre-dried ZrOCl$_2$ · 8H$_2$O (Aldrich, 98%) at 400 °C for 14 hrs under CS$_2$/N$_2$ atmosphere. According to TG/DTA analysis, 4H$_2$O from ZrOCl$_2$ · 8H$_2$O was separated at 98.3 °C and the rest of 4H$_2$O was separated at 153.6 °C. Cl$_2$ from ZrOCl$_2$ was dissociated at 323.7 °C to turn into ZrO$_2$ at 460 °C.

The phase of product was confirmed by using powder x-ray diffractometer (Siemens D500) equipped with mono-chromatized Cu Kα radiation. X-ray data were analyzed using Rietveld-type full-profile refinement technique with a measuring step of 0.02 degree in 2θ value and a counting time of 6 seconds.[11] The refinement was used to obtain the scale factor, back ground parameters, thermal parameters, cell parameters, and atomic positions and occupancies. To estimate the chemical composition of the product, combus-tion analysis was carried out by heating the product at 850 °C until the weight of ZrO$_2$ was fixed after it changed into ZrO$_2$ and SO$_2$. The composition change was observed after heating the sample to higher temperature (~1200 °C).

The powder samples were pressed into cylindrical pellets (approximately 1.3 cm in diameter) under a pressure of 400 kg/cm^2 and coated with gold on both sides. Then the measurements of capacitance, loss, and impedance were performed between 50 Hz and 1 MHz using HP 4284 LCR meter in temperature range -170 to 20 °C which was cont-rolled by liquid nitrogen and temperature controller (Lake-Shore Cryotronic, Inc.). The measurements at above 20 °C were not made because part of the sulfur in ZrO$_x$S could be lost and pure single relaxation by Zr-S and/or Zr-O would not be observed at above 20 °C because of their relaxation-

coupling.

For the ZrO_2 film preparation, Pt substrate was purchased from Inostek Corp. as a Pt film grown on the Ti adhesion layer-SiO_2 adhesion layer-(100) Si wafer. The Pt substrate was primed with the hydroxide layer of 5 wt% 2-mercapto-ethanol/ethanol solution. 100 mM zirconium butoxide solution (3 : 1 ethanol/toluene) was dropped on the hydroxyl terminated substrate, spinned, immersed in pure water for 2 min. to produce ZrO_2 film by hydrolysis, dried with pure nitrogen gas, and annealed slowly at 770 °C for 15 min. after obtaining multilayer. Thickness of the film was measured with α-step (Utencor Instr.). Then gold was deposited on the film using the mask designed to have several electrode holes with 300 μm in diameter size.

The dielectric constant was estimated from the capacitance data using the equation $k = Cd/(k_0A)$,

where k_0 is the permittivity of free space, 8.854×10^{-12} F/m, C is capacitance, d is thickness of the pellet or film, and A is the area of gold plate.

Results and Discussion

The space group of the cubic ZrOS is known to be $P2_13$ with cell dimension of a = 5.696(2) Å[3]. Also the tetragonal one in space group of P4/nmm with cell dimensions of a = 3.55 Å and c = 6.31 Å is known as the alternative phase of ZrOS, and it is a isostructure of PbFCl-type which is a layered structure with Cl-Cl van der Waals interactions between layers.[12]

In the cubic ZrOS cell, Zr atom is coordinated by four sulfurs and three oxygens, where the bond distance of three Zr-S is 2.721(2) Å and that of the other Zr-S is 2.599(2) Å. The Zr atom is located at the center of a distorted mono-capped-octahedron consisting of three oxygens and three sulfurs with the fourth sulfur being capped above the center of the trigonal face formed by three oxygens.

The compound prepared in this research has nonstoichiometric composition which is similar structure but somewhat distorted from the stoichiometric cubic phase. Thus general x-ray pattern of the compound is similar to that of cubic ZrOS except peak splitting and weak extra peaks. Possible tetragonal and orthorhombic lattice types were tried to index all the peaks, and reflection conditions were also considered to determine the space group. Finally, orthorhombic lattice of $P2_12_12_1$ space group with cell dimensions of a = 5.110(2) Å, b = 5.110(7) Å, and c = 5.198(8) Å, *i.e.*, pseudotetragonal structure, gave the best refinement results. No extra peaks except the calculated pattern were observed and relative peak intensities fitted well. Figure 1 shows the x-ray diffraction profiles of ZrO_xS which are calculated and observed. According to the results obtained from Rietveld-type refinement, the structure is distorted from cubic to pseudotetragonal lattice, that is, a structural distortion to low symmetry is made due to the defects on some lattice sites of the stoichiometric cubic structure. The orthorhombic $P2_12_12_1$ space group is a subgroup of the cubic $P2_13$ space group and two three-fold symmetries are broken in the subgroup.
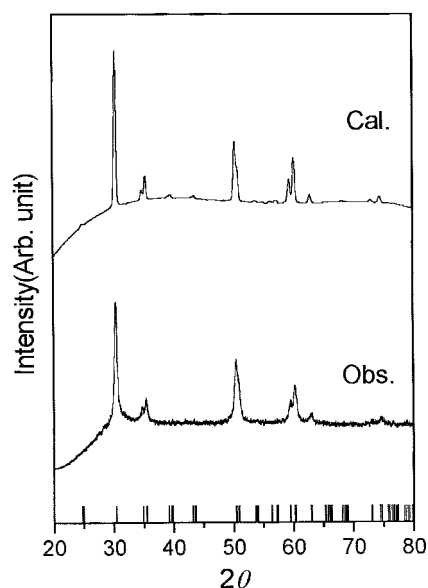

Figure 1. The x-ray diffraction profile of ZrO_xS (x = 0.75). Solid lines represent the calculated (top) and observed (bottom). Vertical strokes indicate calculated Bragg peak positions.

Reduction of orthorhombic cell volume is caused by the existence of defects in stoichiometric ZrOS. The combustion analysis showed that the composition of the sample was $ZrO_{0.75}S$, which is in good agreement with the data of occupancy obtained from final refinement. Since no partial occupancy for sulfur site is indicated within standard deviation in Reitveld analysis, the composition of the sample is assumed to be ZrO_xS. Then the x value in ZrO_xS can be determined by heating it in air as follows:

$$ZrO_xS + [2-(x/2)]O_2 \Rightarrow ZrO_2 + SO_2$$

The positions and occupancies of three atoms, Zr, S, and O composing orthorhombic cell are listed in Table 1, where R_p and R_{wp} are profile R factor and weighted profile R factor.

From the reduction of cell dimension in orthorhombic phase, the bond shortening of Zr-O and Zr-S can be expected

Table 1. Refined parameters for ZrOS in orthorhombic $P2_12_12_1$ unit cell

Atom	Position (x, y, z)	Occupancy (%)
Zr	0.2576(5), 0.2593(5), 0.2636(4)	100
S	0.5329(9), 0.5234(3), 0.5327(0)	100
O	0.8563(9), 0.8650(7), 0.8989(1)	75

R_p = 2.90%, R_{wp} = 3.62%. Cell parameter: a = 5.110(2) Å, b = 5.110(7) Å, c = 5.198(8) Å

Table 2. Bond lengths for orthorhombic $ZrO_{0.75}S$ and cubic ZrOS

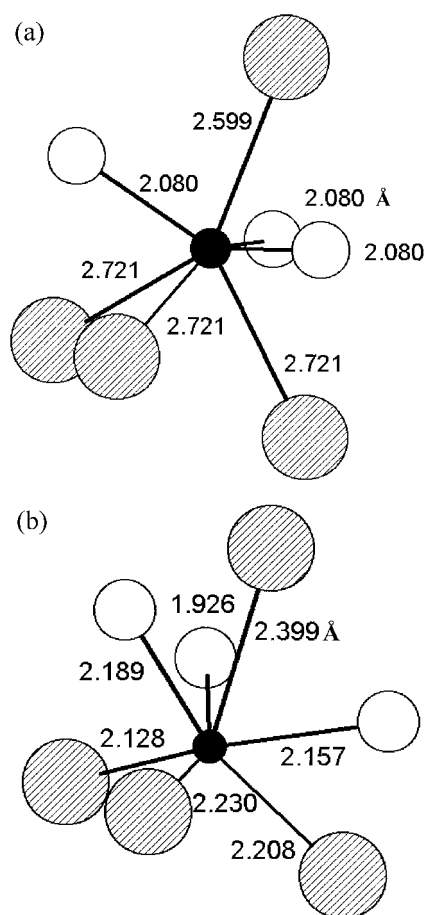| Bond	Orthorhombic (Å)	Cubic (Å)
Zr-O	1.926-2.189	2.080
Zr-S	2.128-2.399	2.599-2.721
Zr-Zr	3.550-3.740	3.590

Figure 2. The coordination and bond distances of Zr cation in (a) cubic ZrOS and (b) orthorhombic ZrO$_{0.75}$S. Filled circle is Zr, dotted circle is S, and open circle is O atom.

as shown in Table 2. Comparing with the cubic ZrOS, Zr atoms in orthorhombic cell are also coordinated by four sulfurs and three oxygens as displayed in Figure 2 with short bond distance of Zr-S and Zr-O. Therefore, some vacancies in oxygen site are stabilized by reducing the inter-anionic repulsion between oxygen and sulfur.

The alternation of Zr-Zr distance of 3.550 and 3.740 Å on ac plane is observed in orthorhombic phase. The shorter Zr-Zr bonds are extended in zigzag mode to the a direction as presented in Figure 3 although there is only one Zr-Zr length in cubic one resulting in isotropic structure in terms of Zr-Zr distance of 3.590 Å. The lattice distortion in ZrO$_{0.75}$S is presumably related to d-electron concentration on Zr site. In stoichiometric ZrOS, the oxidation state of Zr is +4, therefore there are no electrons in d-orbital. However, in ZrO$_{0.75}$S the average oxidation state of Zr is +3.5 with d$^{0.5}$ is possible.

Figure 4(a) and (b) show the dielectric constant and loss (tangent of phase angle) of ZrO$_{0.75}$S at 1 kHz, 10 kHz, and 100 kHz in temperature range -170 to 20 °C. The loss peak can be observed with a sudden change of dielectric constant, which reflects the structural change at corresponding temperature. The dielectric transition at 1 kHz and the shift of the transition toward the higher temperature as measuring
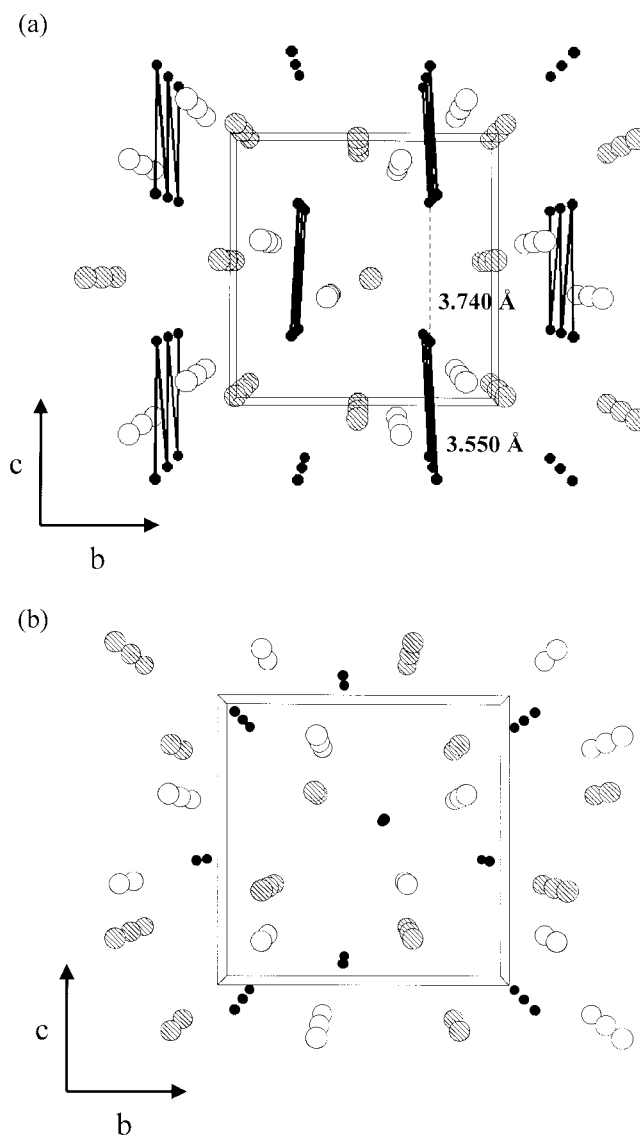

Figure 3. (a) The structure of pseudotetragonal ZrO$_{0.75}$S projected along a direction, where the shorter Zr-Zr bonds are connected as solid lines. Filled circle is Zr, gray circle is S, and open circle is O atom. (b) The structure of cubic ZrOS.

frequency increases can be found in the figure. This transition will be related to the fluctuation of Zr-S or Zr-O in ZrO$_{0.75}$S. The dielectric property of monoclinic ZrO$_2$ bulk which is coordinated with 7 oxygen atoms was also measured with temperature to get information about the Zr-O fluctuation. No sudden change in dielectric constant was obtained from -150 °C to -20 °C except at 20 to -10 °C indicating that the increase of dielectric constant of ZrO$_{0.75}$S at -70 °C is due to fluctuation of Zr-S segment. In addition, Zr-S bond is longer (weaker) and more polarizable than those of Zr-O, which reflects a rapid increase of dielectric constant and loss at low temperature, -70 °C. Actually, the variety of bond length in each Zr-S and Zr-O will make the dielectric situation more complicate at above -20 °C.

The magnitude of dielectric constant, 200.2 at 100 kHz and at 20 °C is much higher than those of bulk and thin film
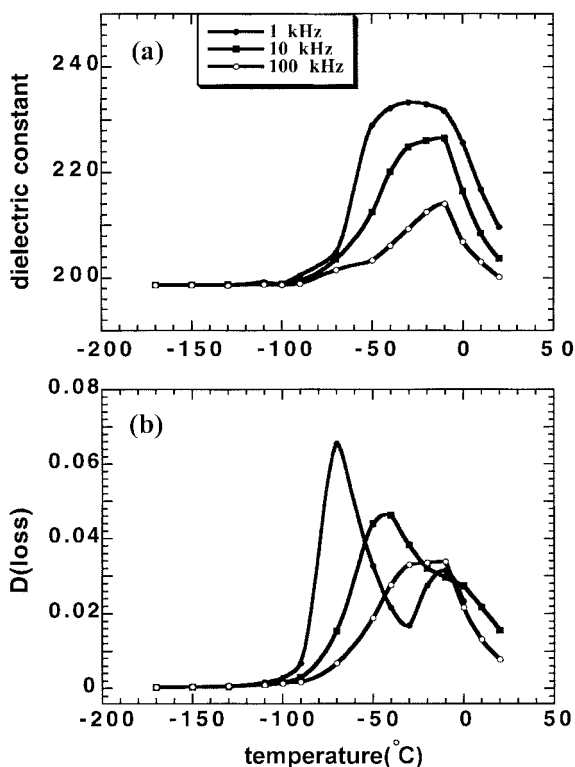
Figure 4. (a) dielectric constant and (b) loss of $ZrO_{0.75}S$ at 1 kHz, 10 kHz, and 100 kHz in temperature range -170 to 20 °C.
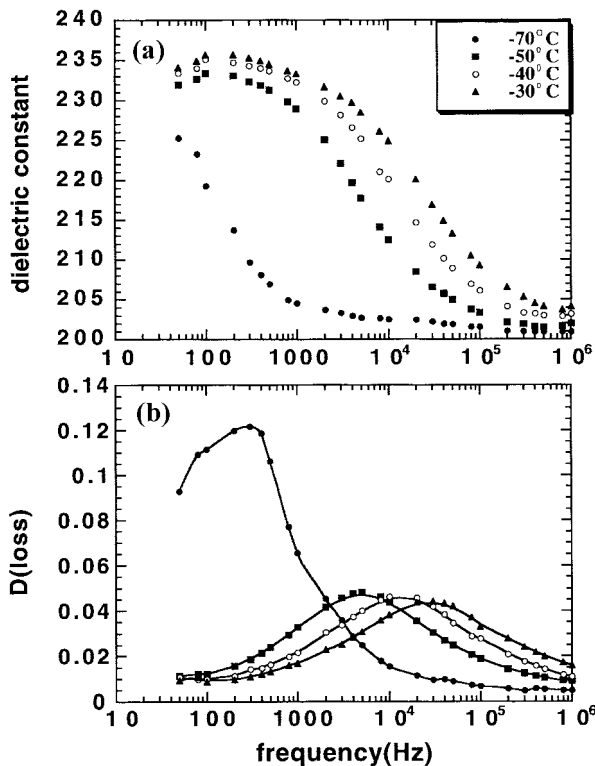

Figure 5. (a) dielectric constant and (b) loss curves of $ZrO_{0.75}S$ with frequency at -70 to -30 °C. The shift of the relaxation to high frequency can be observed as temperature increases.

ZrO_2, 9.0-7.9, confirming more polarizable $ZrO_{0.75}S$ system. ZrO_2 film is substantially less dense than bulk oxide because

cracks appear on the film during contraction process, which results in lower dielectric behavior than bulk ZrO_2 even though annealing produces dense and adherent film than as-prepared film.[13] The dielectric studies on thin film will be discussed in other paper in detail. Not only the structure, but also the low loss and high resistivity of $ZrO_{0.75}S$ reveal that its electric system is so different from semiconducting ZrS_2, confirming that $ZrO_{0.75}S$ can be a proper candidate as a dielectric at room temperature.

The single relaxation of Zr-S in frequency range 50 Hz to 1 MHz at -70 to -30 °C can be found in Figure 5. Dielectric constant and loss peak curves in Figure 5(a) and (b) move to higher frequency as temperature increases indicating that the dielectric relaxation of Zr-S shifts to higher frequency with temperature. The relaxation frequency of dielectric absorption maximum, f_{max}, is expressed as

$$2 \pi f_{max} t = 1.$$

Thus f_{max} obtainted experimentally can be used to determine the relaxation time, τ. The shifting factor, a(t), is the ratio of relaxation time at a certain temperature, τ_t, to the relaxation time at reference temperature, τ_r, as

$$a(t) = \tau_t / \tau_r .$$

At reference temperature the shifting factor, a(t), equals to 1. Relaxation time and shifting factor at each temperature is compared with that at reference temperature, -50 °C, in Table 3. Using the Arrhenius relation,

$$\tau_t = \tau_0 \exp(E_a / RT)$$

where E_a is activation energy of the relaxation time which is independent of absolute temperature, T, in single relaxation.[14] Thus

$$\ln \tau_t = \ln \tau_0 + E_a / RT_t,$$
$$\ln \tau_r = \ln \tau_0 + E_a / RT_r,$$

and

$$\ln a(t) = (E_a / R) (1/T_t - 1/223), \text{ where } T_r \text{ is } 223 \text{ K } (= -50 \text{ °C}).$$

Therefore, by plotting the curve of ln a(t) as the function of $1000(1/T_t - 1/223)$ as shown in Figure 6 the activation energy of relaxation time of Zr-S, 0.47 eV (11.3 kcal/mole) can be estimated from the slope.

Z′ and Z″ in Figure 7 are real part and imaginary part of the complex impedance. When the a.c. (alternate current) data is plotted on a impedance plane, the data usually take the form of semi-circles and/or spikes. The series circuit of R (resistance) and C (capacitance) gives a vertical spike in

Table 3. Relaxation time and shifting factor of Zr-S

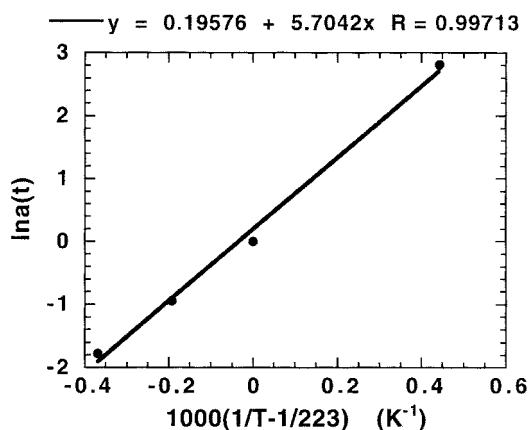| Temperature (°C)	τ_t	a (t)
−70	5.31×10^{-4}	16.67
−50	3.18×10^{-5}	1.00
−40	1.22×10^{-5}	0.38
−30	5.31×10^{-6}	0.17

Figure 6. ln a(t) as the function of 1000(1/T-1/223), where the a(t) is shifting factor and T is absolute temperature.
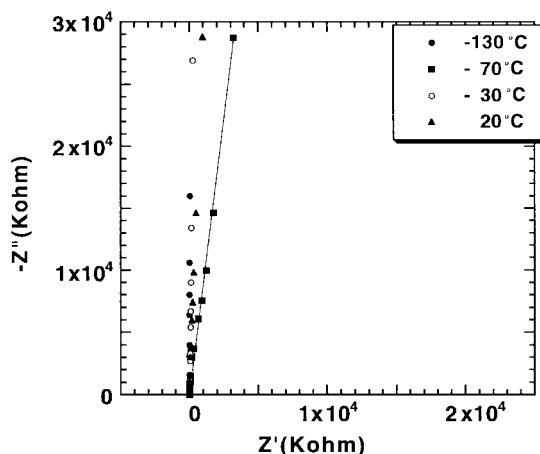

Figure 7. Complex impedance spectra of ZrO$_{0.75}$S at several temperatures. Solid line represents the impedance curve at -70 °C.

the plane because Z′ is of fixed value, R, and Z″ decreases with increasing frequency. On the other hands, the parallel R and C circuit gives rise to a semi-circle. In this case, Zr-S relaxation observed at -70 °C causes some part of inherent resistance in parallel to the capacitance. At the other temperatures except -70 °C, nearly the forms of spike are observed, proposing more series RC circuit character apparently.

References

1. Conroy, L. E.; Park, K. C. *Inorg. Chem.* **1969**, *7*, 459.
2. Hauser, O. *Z. Anorg. Chem.* **1907**, *53*, 74.
3. McCullough, J. D.; Brewer, L.; Bromley, L. A. *Acta Cryst.* **1948**, *1*, 287.
4. Jellinek, F. *Acta Chem. Scand.* **1962**, *16*, 791.
5. Wold, A.; Dwight, K. *Solid State Chemistry*; Chapman and Hall, Inc.; New York, 1993; p 106-111, p 183.
6. Vest, R. W.; Tallan, N. M.; Tripp, W. C. *J. Am. Cer. Soc.* **1964**, *47*, 635.
7. Whitney, E. D. *J. Electrochem. Soc.* **1965**, *112*, 91.
8. Tributsch, H. *J. Electrochem. Soc.* **1981**, *128*, 1261.
9. Conroy, L. E.; Park, K. C. *Inorg. Chem.* **1968**, *7*, 459.
10. (a) Ichinose, I.; Senzu, H.; Kunitake, T. *Chem. Mater.* **1997**, *9*, 1296. (b) Ichinose, I.; Kawakami, T.; Kunitake, T. *Adv. Mater.* **1998**, *10*, 535.
11. Sakthivel, A.; Young, R. A. *Program DBW006PC for Reitveld Analysis of X-ray and Neutron Powder Diffraction Pattern*, 1990.
12. Wells, A. F. *Structural Inorganic Chemistry*; Clarendon Press: Oxford, 1984; p 487.
13. Fang, M.; Kim, C. H.; Martin, B. R.; Mallouk, T. E. *J. Nanopar. Res.* **1999**, *1*, 43.
14. McCrum, N. G.; Read, B. E.; Williams, G. *Anelastic and Dielectric Effects in Polymeric Solids*; Dover Publications, Inc.: New York, 1991; p 119.